Nanoscale

Accepted Manuscript

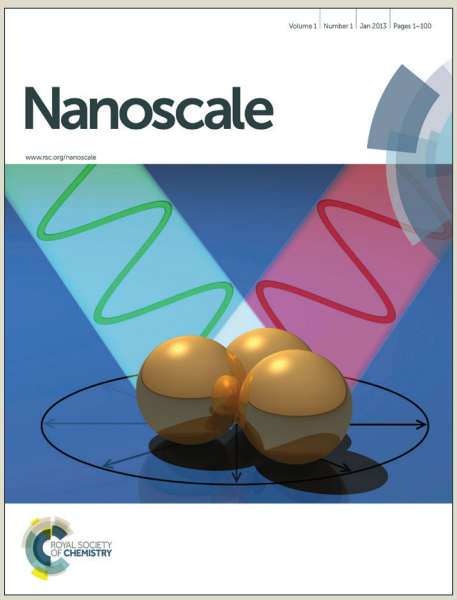

ROYAL SOCIETY OF CHEMISTRY

www.rsc.org/nanoscale

Nanoscale

RSCPublishing

ARTICLE

An NIR-Triggered and Thermally Responsive Drug Delivery Platform through DNA/Copper Sulfide Gates

Cite this: DOI: 10.1039/x0xx00000x

Lei Zhang,[a] Yecheng Li,[b] Zexun Jin [a], Jimmy C. Yu[a#] and King Ming Chan[b]

Received 00th January 2012,
Accepted 00th January 2012

DOI: 10.1039/x0xx00000x

www.rsc.org/

Nanomaterials for effective drug delivery require zero pre-release and on-demand release of therapeutic drugs. In this work we demonstrate a novel drug delivery system composed of a mesoporous silica platform conjugated to CuS nanoparticles with two complementary DNA sequences. CuS nanoparticles act as both gatekeepers preventing pre-release of drugs and photothermal agents for effective killing of cancer cells. This system exhibits temperature and NIR- responsive DOX release, with additional accelerated release rate with GSH treatment. Therefore, it can act as an effective anticancer drug delivery carrier with triggered drug release and efficient anti-cancer effect *in vitro* after NIR irradiation.

Introduction

The use of nanoparticles as drug delivery systems for on-demand release of therapeutic agents has attracted much attention in recent years. Nanoparticle systems with high loading efficiency, targeted delivery and controlled release of drugs can greatly enhance the therapeutic effect. External stimuli that have been exploited for controlled release include redox,[1-3] pH,[4-6] light,[7-13] enzymes,[14-16] magnetic field,[17, 18] glucose[19] and ultrasound.[20, 21] Among these, near-infrared (NIR, λ = 700–1100 nm) light is considered an effective tool in photothermal therapy. An unique advantage of NIR is its deep penetration of but minimal absorbance in normal tissues.[22]

The NIR irradiation would not only trigger the drug release, but also enhance the chemotherapy efficiency by its property and endocytic disruption. After entering cells, nanoparticles must be able to escape the endosome or lysosome before delivering their therapeutic effects. Researchers have shown that photothermally induced heat may help to disrupt the endosome, allowing the payload to diffuse into the cytosol.[23, 24] If they carry photosensitizers, photodynamic therapeutic results can be achieved.[25] Those results strongly support the feasibility of designing NIR-induced drug delivery systems.

Copper sulfide (CuS), a well-known p-type semiconductor material, has recently emerged as a new photothermal ablation agent in photothermal therapy. CuS nanoparticles (NPs) have advantages such as a low cost, low cytotoxicity and their intrinsic NIR absorption derived from energy band transitions instead of surface plasmon resonance. Li *et al.* and Chen *et al.* synthesized CuS nanospheres of 5 nm and 11 nm, respectively.[26, 27] They conducted photothermal ablation using an 808 nm laser. Hu and co-workers prepared flower-like CuS superstructures as 980 nm laser-driven photoblation agents, in which the 980 nm laser had better penetration and photothermal effects.[28]

Drug delivery vehicles for NIR-triggered release are mainly composed of NIR absorption agents and a drug-containing moiety. The dual effects of photothermal ablation and chemotherapy could provide efficient synergistic therapeutic treatment for cancer cells. In some examples, nanomaterials are both drug-containing and NIR-absorbing, including gold nanocages,[29, 30] graphene nanosheets[31, 32] and hollow copper sulfide nanoparticles.[33, 34] Despite their effectiveness, the combination of different materials into a nanocomposite structure brought irreplaceable advantages as thermally-responsive drug carriers, such as higher loading capability, less pre-release and easier functionalization. Specifically, the mesoporous silica nanoparticle (MSNs) has been chosen as the drug loading platform due to its commonly known biocompatibility, mesoporous structure, large surface area and tunable pore sizes and volumes,[35-37] while the toxicity issues of CuS NPs has been less studied in biological systems. Second, the easy functionalization and high loading capability of MSN make it a more suitable drug carrier with the stimuli-responsive release property. Two recent examples of nanocomposites incorporated MSN and CuS nanoparticles as multi-functional chemo-photothermal therapy for cancer cells.[38, 39] In both cases, DOX was loaded into MSNs and CuS acted as photothermal agents as well as gatekeepers from pre-release of DOX. These nanohybrids exposed synergistic anti-cancer effect, with higher cancer cell killing efficiency than any of the single approaches alone.[40]

In this study, a smart photothermally controllable drug delivery system was synthesized with MSN and CuS nanospheres. Different from previous studies on CuS-coated MSNs, in our case, the CuS NPs were not attached to MSNs via electrostatic interactions, but through two complementary oligonucleotide sequences. This unique design provides reversible opening-closing effect while the temperature changes. The CuS NPs played the role of the capping, photothermal and photoablation agent. When irradiated with an NIR laser, the localized heat generated made the DNA duplex de-hybridize and the DOX release. The detached CuS NPs also acted as a photoablation agent. The synergistic effect from

NIR-triggered DOX release and photothermal ablation is a promising approach in the treatment of cancer cells, especially drug-resistant cells.

Experimental

Materials

Reagents $CuCl_2 \cdot 2H_2O$ and thioacetamide were purchased from Ajax Finechem (Thermo Fisher Scientific) and Merck, respectively. Sodium hydroxide (NaOH), thioglycolic acid, tetraethyl orthosilicate (TEOS), (3-aminopropyl)triethoxysilane (APTES), tris(2-carboxyethyl)phosphine (TCEP), N-hydroxylsulfosuccinimide (NHS) and 1-ethyl-3-(3-dimethylaminopropyl) carbodiimide (EDC) were purchased from Sigma-Aldrich. Succinimidyl 4-*N*-maleimidomethyl cyclohexane-1-carboxylate (SMCC) was purchased from Thermo Scientific. Fluorescein isothiocyanate (FITC) was obtained from Analytical Reagents. The thiol-modified oligonucleotides, 5'-thiol C6-TTATCGCTGATTCAA and the amine-modified complementary sequence 5'-amine C6-TTGAATCAGCGATAA, were purchased from GenScript, Inc (Nanjing, China), as well as the oligonucleotide tagged with a fluorescein probe ([Flc]TTGAATCAGCGATAA). HeLa cells (a human cervix carcinoma cell line) were obtained from the American Tissue Culture Collection. Fetal bovine serum (FBS), Dulbecco's modified Eagle's medium (DMEM) and penicillin-streptomycin were obtained from GIBCO.

Characterizations

The size and morphology of nanoparticles were examined by transmission electron microscopy (TEM) using a Tecnai™ Spirit microscope (FEI, Japan). The hydrodynamic sizes were analyzed with Nanosight NS 500 (Malvern, UK). FTIR and UV-Vis-NIR absorbance spectra were measured with Nicolet 670 (Thomas Nicolet) and U-3501 (Hitachi) spectrometer, respectively.

Methods

Preparation of thioglycolic acid-stabilized CuS NPs. CuS NPs were prepared by minor modification of a procedure reported previously.[26] Briefly, 0.1 mmol $CuCl_2 \cdot 2H_2O$ was dissolved in a three-necked flask containing 100 mL distilled water, then 0.2 mmol TGA was added to the solution. The pH of the solution was adjusted to 9.0 by the addition of 1 M NaOH and the system was degassed by nitrogen bubbling for 20 min. After the addition of 20 mL distilled water with 0.1 mmol thioacetamide, the solution was heated at 50°C for 3 h. The desired CuS NPs were centrifuged, washed with acetone and dispersed in autoclaved deionized water at a certain concentration.

Synthesis of amine-functionalized MSN (MSN-NH_2). The synthetic procedure followed the modified Stöber method, using cetyltrimethylammonium bromide (CTAB) as the structure-directing agent under basic pH conditions.[41] CTAB (100 mg) was added to 100 mL deionized H_2O with 3 mL $NH_3 \cdot H_2O$ (28%) and 0.5 mL TEOS. The solution was vigorously stirred for 30 s and left overnight. The precipitate was centrifuged and washed with deionized water. For FITC-labeled MSN, 1 mg FITC was first reacted with 2.5 μL (3-aminopropyl)triethoxysilane (APTES) in 0.5 mL ethanol for 2 h in the dark. The FITC-labeled APTES was mixed with 0.5 mL TEOS and added to the solution. To remove the template, the dried powder was heated to 425°C in air and calcined for 3 h, or refluxed in ethanol containing HCl for 6 h. The template-free mesoporous material (100 mg) was degassed under vacuum before being reacted with 1.34 mmol APTES in toluene under an N_2 atmosphere for 16 h. The products were filtered, washed with toluene and dried under vacuum.

Oligonucleotide immobilization on MSN-NH_2 and CuS. The thiol-modified oligonucleotide (20 nmol), 5′-thiolC6-TTATCGCTGATTCAA, was first treated with 0.1M TCEP for 30 min to reduce its disulfide bonds and ensure its activity. G-25 Sephadex columns (GE Healthcare) were used to purify the reduced thiolated products. DNA coupling to MSN-NH_2 was carried out with SMCC as a cross-linker. SMCC and 10 mg MSN-NH_2 were reacted for 2 h in 5 mL tetrahydrofuran. After centrifugation and washing to remove excess cross-linker, the SMCC-activated MSN were suspended in 5 mL 0.1 M PBS buffer, 0.2 M NaCl (pH 7.2). The purified thiol-DNA was added and reacted overnight. The DNA-immobilized MSN (MSN-DNA) was then washed three times in 10 mM Tris-HCl, 150 mM NaCl, and 0.05% Tween 20 buffer (pH 7.5). The amount of attached DNA was estimated by subtracting the DNA accumulated in the supernatant and washing solutions from the total DNA, measured by a Cary 300 UV-Vis spectrometer (Agilent Technologies). The complementary oligonucleotide sequence, 5′-amine C6-TTGAATCAGCGATAA, was used for DNA coupling to CuS NPs. CuS NPs (10 mg) was activated with an excess of NHS/EDC for 30 min, centrifuged and washed to remove the unreacted crosslinker. The amine-oligonucleotide (20 nmol) was added and reacted overnight. The washing steps and attached DNA estimation were performed as for the MSN-NH_2. Both DNA conjugates were dispersed in a buffer containing 20 mM Tris-HCl and 37.5 mM $MgCl_2$ (pH 8.0) for subsequent hybridization.

DNA hybridization. To prove the reversible hybridization/dehybridization mechanism of the selected DNA sequence, the oligonucleotides were tagged with a fluorescein probe ([Flc]TTGAATCAGCGATAA) and hybridized with DNA-conjugated MSN. Both species were mixed in an orbital shaker at 120 rpm for 3 h, producing MSN-DNA-Flc. In the CuS NP gated MSN system for controlled DOX release, DNA-coupled MSN were soaked in concentrated DOX (10 mg/mL). The mixture was stirred at room temperature for 24 h to reach equilibrium state. Then the unabsorbed DOX molecules were washed out by centrifugation at 12 000 rpm for 10 min. The loading amount of DOX was determined with UV-Vis spectroscopy by subtracting the original and remaining DOX concentrations and calculated by the following equation.

$$Loading\ amount\ (\mu g/mg) = \frac{Weight\ of\ drug\ in\ MSNs}{Weight\ of\ loaded\ MSNs}$$

The DNA-coupled MSN loaded with DOX were mixed with DNA-tagged CuS NPs in hybridization buffer at 120 rpm for 3 h. The product (MSN-DNA-CuS) was intensively washed with deionized water to remove the unabsorbed CuS NPs. The UV-Vis-NIR absorbance of the CuS NPs and synthesized MSN-DNA-CuS solutions were measured with a U-3501 UV/VIS/IR spectrometer (Hitachi, Japan). The atomic ratio between Cu and Si in the MSN-DNA-CuS was determined with an inductively-coupled plasma optical emission spectrometer (ICP-OES).

Fluorescein and DOX release assays. To investigate the hybridization/dehybridization process of MSN-DNA-Flc and the DOX release kinetics of MSN-DNA-CuS, a certain amount of each complex was put into separate cuvettes with 0.1 M PBS (pH 7.4). The temperature change was conducted with a water bath incubator. The fluorescein and DOX release in the

supernatant solutions was measured with a Cary 300 UV-Vis spectrometer at different time points and temperatures (Agilent Technologies).

Cell culture and the photothermally controlled drug effect of NIR irradiation *in vitro*. HeLa cells (human cervical cancer cells) and MCF-7 cells (human breast adenocarcinoma cells) were grown at 37°C in 5% CO_2 in DMEM supplemented with 10% FBS, 100 units/mL penicillin and 100 μg/mL streptomycin. The anticancer effect caused by both the photoablation and photothermally controlled DOX release of MSN-DNA-CuS was evaluated using AlarmaBlue assay. The same concentration of CuS NPs as contained in the MSN-DNA-CuS was used as the control. The cells were seeded onto 96-well plates at a density of 1×10^4 cells/well and incubated for 24 h. The cells were exposed to two concentrations (2.5 and 5.0 ppm or μg/mL CuS; ppm indicates μg/mL in all of the following studies) of the two nanoparticles for 3 h in 100 μL of serum-free media. The cells were then irradiated with a 980 nm laser at a power density of 4 W/cm^2 for 0 to 30 s, followed by incubation for 24 h. The cell medium was replaced with 100 μL fresh medium containing 10% AlarmaBlue and incubated for another 2 h. The absorbance was measured at ex 560 nm/em 590 nm using a microplate reader (Tecan Infinite M200). To better elucidate the toxic effect of the nanoparticles, CuS and MSN-DNA-CuS without DOX were also added to the HeLa cells in a 96-well plate for comparison. Different amounts of DOX alone were added for comparison. Cells incubated with these three controls were not irradiated with NIR. The cytotoxicity was evaluated after 24 h using the AlarmaBlue assay, as indicated above. Experiments were conducted in triplicates and significant differences were analyzed by using PRISM software 6.0.

Confocal laser scanning microscope study. One day before the experiment, 10^5 HeLa cells were seeded in a confocal dish 34.3 mm × 9.3 mm (SPL, Korea). The cells were incubated with MSN-DNA-CuS containing DOX (FITC-labeled MSN) at 37°C. Live cell imaging of nanoparticle uptake and DOX release was performed using a Nikon C1si confocal laser scanning microscope equipped with a spectral imaging detector (Nikon, Japan) and an INU stage-top incubator (Tokai Hit, Japan) at 1 h and 3 h after exposure. FITC and DOX were excited at 488 nm and 532 nm. The corresponding emission spectra were 500-530 nm and 560-660 nm, respectively. The spectral data were analyzed using the Nikon EZ-C1 software. After exposure to MSN-DNA-CuS containing DOX for 1 h, the HeLa cells were irradiated with the 980 nm laser at a power density of 4 W/cm^2 for 30 s to compare NIR irradiation to DOX release *in vitro*. Images were taken at the same settings before and after NIR irradiation. The signal intensity of DOX was compared to calculate the amount of DOX released.

Flow cytometric analysis. HeLa cells were seeded in 24-well culture plates (2×10^4 cells/well) for 24 h before the addition of MSN-DNA-CuS. Three hours later, the cells were irradiated with the 980 nm laser at a power density of 4 W/cm^2 for 0-60 s. Before harvesting, the cells were washed three times with PBS to remove the loosely attached nanoparticles. Then the cells were incubated with 100 μL 0.25% trypsin/EDTA for 10 min at 37°C for detachment. The harvested cells were centrifuged and the supernatant was removed and suspended in ice-cold PBS supplemented with 2% FBS. The cellular uptake of the different components was assayed by flow cytometry using a FacsCanto flow cytometer (Beckman Coulter, USA). DOX was excited at 536 nm and emitted at 585/42 nm. To exclude dead cells and debris, the samples were gated by forward/side scattering and 10^4 events per sample were collected. The data were analyzed with the software FlowJo 7.6.1.

Results and discussion

Synthesis and characterization of MSN-DNA-CuS

MSN was chosen as the drug-loading vehicle as it has a higher surface area than solid particles. The average MSN was about 70-120 nm, which is considered the proper size for nanoparticle internalization and circulation *in vivo*.[42] The coupling of DNA to MSN and CuS was mediated with EDC/NHS as the linker for amide bonds. The construction of the DOX-containing and CuS-capping vehicle is summarized in Scheme 1.

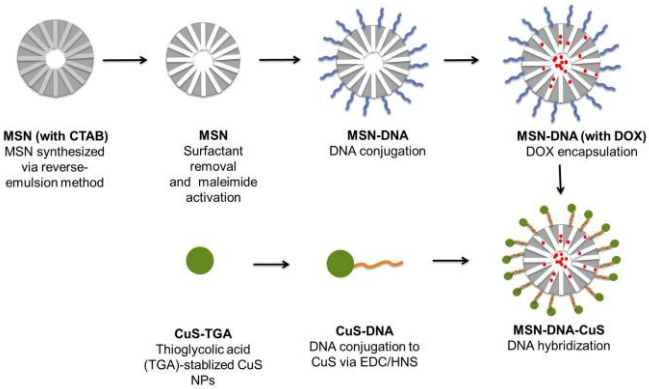

Scheme 1. Graphic scheme for the synthesis of MSN-DNA-CuS

The sizes and mesoporous network can be clearly seen in the transmission electron microscopy (TEM) images in Fig. 1a. The hydrodynamic size distributions of MSNs before and after CuS conjugation were also investigated in PBS buffer (pH=7.4). As shown in Fig. 2, CuS conjugation increased the hydrodynamic sizes of MSNs from ~140 nm to ~ 200 nm. The enhanced size was due to some aggregated small CuS NPs on the surface of MSNs. Reaction with APTES changed the isoelectric point of MSN, which was supported by the zeta potential of MNS-NH_2 in distilled water, measured to be +37.47 mV (Fig. 1d). After coupling to thiol-DNA, the zeta potential of the MSN-DNA decreased to +23.88 mV, as it was affected by the negatively charged oligonucleotide.

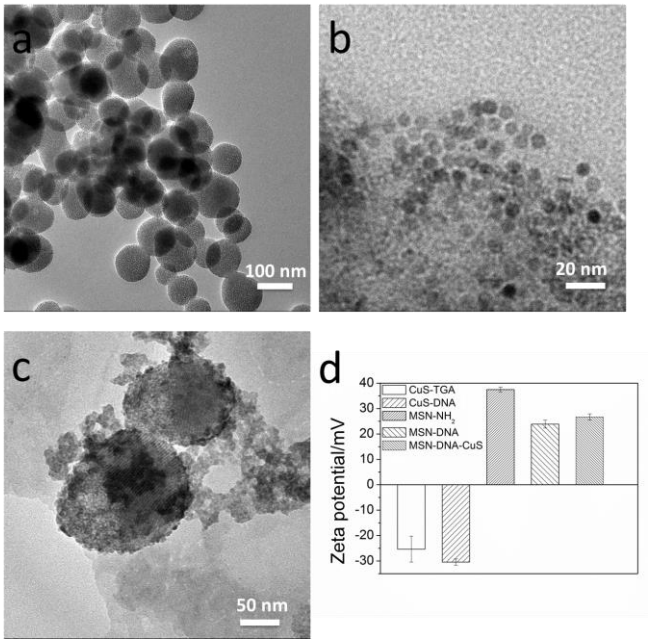

Fig.1 TEM images of (a) MSN, (b) CuS, (c) MSN-DNA-CuS and (d) the zeta potentials of the synthesized nanoparticles before and after DNA immobilization and CuS complexion.

The zeta potential of the TGA-stabilized CuS NPs in H_2O was negative as -25.33 mV, due to existence of carboxylate from thioglycolic acid on the surface.[43] After conjugation to amine-DNA, the zeta potential changed to more negative in H_2O. After DNA linkage and hybridization of CuS-DNA, the generated complex MSN-DNA-CuS possessed a zeta potential of +26.71 mV. This positively charged complex may be able to physiochemically interact with the negatively charged cellular membrane, making the internalization of MSN-DNA-CuS easier.

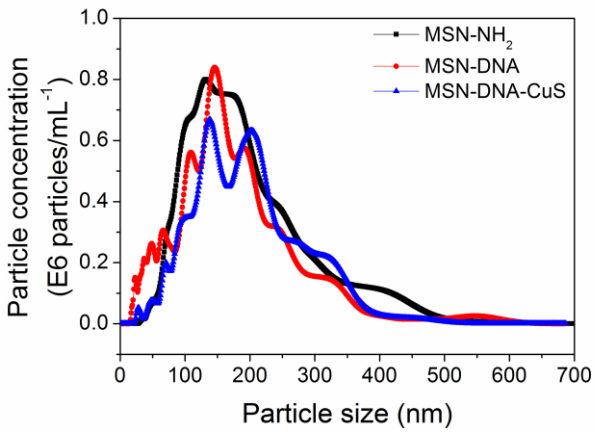

Fig. 2 Hydrodynamic size sitribution profiles of MSN-NH_2, MSN-DNA and MSN-DNA-CuS nanoparticles in PBS (pH=7.4).

The FTIR spectra are shown in Fig. 3. The absorption band at 1562 cm^{-1} was assigned to the bending of N-H from the amine groups modified on MSN. For MSN-NH_2 after conjugation of SMCC (MSN-NH-SMCC), the merging band at 1710 cm^{-1} was due to C=O stretching in the amide bonds formed by the covalent bond between SMCC and MSN. After DNA coupling and DNA hybridization of MSN, the absorption bands from DNA could be assigned as follows according to previous reports:[44-46] the peak at 796 cm^{-1} due to the sugar conformations, 953 cm^{-1} from P-O stretching. These two DNA peaks supported the existence of DNA in the MSN-DNA-CuS complex. The peak around 1225 cm^{-1} due to PO^{2-} asymmetric stretching from the DNA phosphate backbone overlapped with the shoulder peak of Si-O-Si asymmetrical stretching and could not be differentiated. Due to the limited amount of DNA, the corresponding peaks were not very strong. The carboxyl and carbonyl groups of the TGA-capped CuS NPs, at bands 1550 cm^{-1} and 1250 cm^{-1}, could not be differentiated due to overlap with other peaks. However, the TEM image confirmed the existence of the CuS NPs (Fig. 1c).

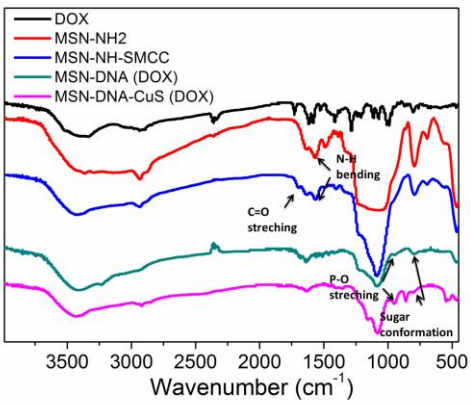

Fig. 2 FTIR spectra of DOX, MSN-NH_2, MSN-NH-SMCC, MSN-DNA (DOX) and MSN-DNA-CuS (DOX) (top to bottom). The representative absorption bands are indicated by arrows.

By referring the work of Ruiz-Hernandez and co-workers,[47] the two complementary sequences with a melting temperature of 47°C were selected as the upper limit of the cancer hyperthermia temperature range. The DNA absorbance was calculated with UV-Vis spectroscopy, showing 50% and 80% anchored DNA on MSN and CuS NPs, respectively. ICP-OES indicated the molar ratio between CuS and SiO_2 in the MSN-DNA-CuS to be about 1.4. The stock solution of 145 ppm MSN-DNA-CuS therefore contained 100 ppm CuS.

The temperature-responsive behavior of MSN-DNA-Flc

The complementary oligonucleotides labeled with a fluorescent probe ([Flc]5'TTGAATCAGCGATAA3') were hybridized with MSN immobilized with thiol-DNA, to confirm the successful immobilization of thiol-DNA on the MSN surface and to investigate the response of DNA molecules hybridized to MSN to temperature changes. A water bath was set to increase to and maintain different temperatures for 15 min, then decrease to and maintain room temperature (25°C) for 15 min. The release of fluorescein-tagged oligonucleotide is shown in Fig. 4.

In the first 240 min, the release of the fluorescein-labeled oligonucleotide increased as the temperature rose, indicating varied degrees of DNA melting. When the temperature was lower than 47°C, the release was not obvious due to little detached DNA and the lagged equilibrium of the DNA in the

supernatant of the cuvette. At higher temperatures, the release rate was much greater, due to the de-hybridization of the DNA sequences. The temperature for DNA de-hybridization is dependent on the melting temperature of the double stranded DNA complex, which is usually affected by the DNA sequence, length and concentration. After each incubation of 15 min at room temperature, the FIFC absorbance decreased a little, due to the partial re-hybridization of the two DNA sequences. Unlike previous reports,[47] the MSN did not completely retain the DNA-Flc. There was incomplete contact between the two components, as the MSN stayed in the bottom of the cuvette. To prove the possibility of re-hybridization, the system was mixed at 120 rpm for 3h and left overnight before measuring the absorbance. More than 90% of the DNA-Flc hybridized and anchored to the MSN surface again.

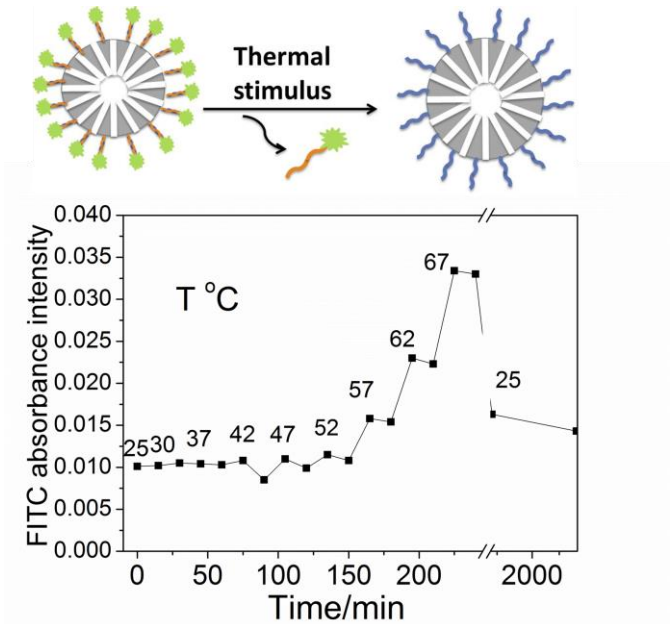

Fig. 4 Above: schematic illustration of the thermally-triggered detachment of fluorescein-labeled oligonucleotide from MSN, and below: the fluorescein-labeled oligonucleotide release profile from the MSN in a time-temperature dependent manner.

The photothermal effect of CuS and MSN-DNA-CuS

The UV-Vis absorption of the TGA-capped CuS aqueous solution was similar to previous reports.[26] In Fig. 5, the short wavelength absorption edged at around 550 nm, which agreed well with the reported value for the band gap (Eg = 1.85 eV) of bulk CuS. The increased absorption in the NIR region was due to inter-band transitions (absorptions) from valence states to unoccupied states.[48] The absorbance intensity of MSN-DNA-CuS was smaller than of CuS, suggesting that silica may block the light and affect the absorption of CuS NPs.

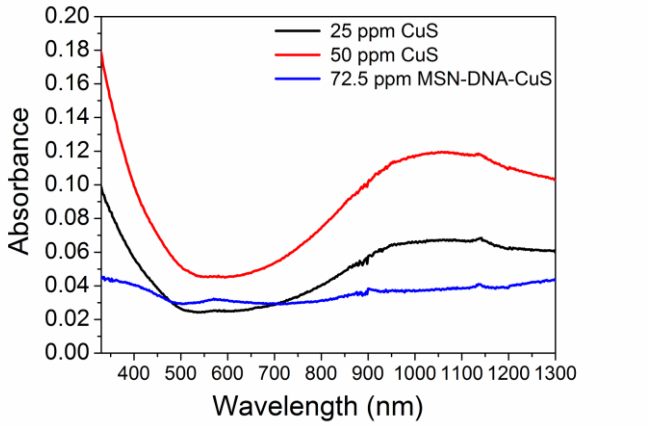

Fig. 5 UV-Vis-NIR absorbance spectrum of 25 ppm and 50 ppm CuS NPs and 72.5 ppm MSN-DNA-CuS in deionized water.

To investigate the photothermal effect of MSN-DNA-CuS, different concentrations (3.625 and 7.25 ppm) of the nanoparticles were dispersed in PBS. The same amount of CuS was used for comparison (2.5 and 5.0 ppm). PBS was used as a blank. The temperature increase after irradiation with the 980 nm laser at a power density of 4 W/cm^2 for 4 min is shown in Fig. 6.

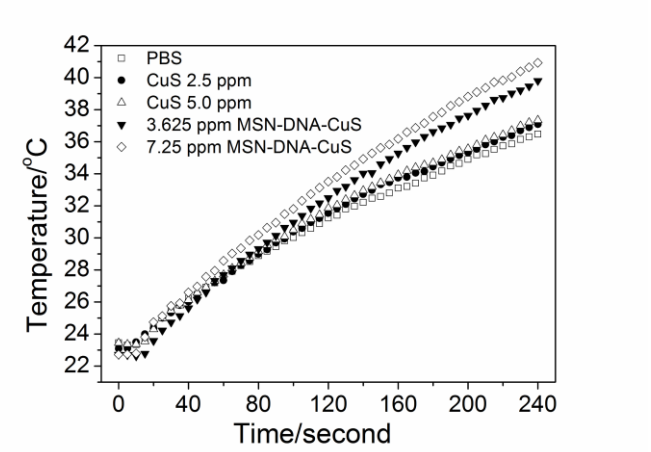

Fig. 6 The temperature increase of PBS containing different concentrations of CuS and MSN-DNA-CuS as a function of irradiation time.

The temperature of the PBS blank increased about 14°C in 4 min. This temperature change was reasonable considering the strong power of the NIR laser and the long irradiation time. The temperature increases of the 2.5 and 5.0 ppm CuS solutions were not significantly different from that of PBS, probably due to the much smaller concentration compared with previous reports.[26, 28] However, the two concentrations of the MSN-DNA-CuS complex, containing 2.5 and 5.0 ppm CuS, used the 980 nm laser energy more effectively. The temperature increased with the increase in nanoparticle concentration and/or irradiation time. In all of the cases, the heating rate slowed with the increase in temperature, due to faster heat loss at higher temperatures.[49] Considering the poor absorption intensity of the complex compared with the CuS NPs, as suggested in Fig. 5, the photothermal conversion was much higher at the same

concentration of CuS NPs. The better photothermal conversion efficiency is attributable to the structure, not the concentration. The TEM images showed the "aggregation" of the CuS NPs on the MSN surface. This generated more localized heat and increased the photothermal conversion efficiency. This effect was similar to that found by Tian and co-workers, who found that the absorption intensity of CuS superstructures was twice that of comparable CuS hexagonal nanoplates.[28]

Stimuli-triggered DOX release of MSN-DNA-CuS

In the process of DOX loading into MSNs, the initial concentration of DOX in the MSN dispersion was much higher than that inside the MSNs. Thus, the DOX would diffuse from the outside to the channels of MSNs driven by the diffusion effect until equilibrium state was reached.[50] Due to the protonation of DOX at pH 7.4 (pKa=8.4[51]) and the presence of silanol groups in MSN, DOX were kept inside MSNs via both electrostatic interactions and hydrogen bonds.[52] The DOX loading ability of MSN-DNA was calculated to be 98.18 mg/g and of FITC-labeled MSN-DNA to be 51.61 mg/g. The FITC labeling may have affected the mesoporous structure and may have interacted with the DOX molecules. A stimuli-responsive DOX release study was performed using non-FITC-labeled MSN to better understand the DOX release profile.

DOX release was monitored by increasing the temperature and time and measuring the DOX concentrated in the supernatant of the cuvette. Thiol-DNA immobilized, uncapped MSN (MSN-NH-DNA) was used as a control after DOX loading. Fig. 7a shows that the DOX release from the non-capped MSN followed the typical release pattern associated with mesoporous matrices without capping.[53] Fig. 7b shows that the DOX release from the capped system was exponential and temperature-dependent. The differences indicated that DNA conjugation was not able to stop drug release and confirmed the successful capping of the CuS NPs in the MSN. Comparison of the DOX release percentage showed that the release was much more rapid in the uncapped system than in the capped system. It may have taken time for the CuS to detach from the MSN surface. The incomplete removal of CuS NPs may have slowed down the DOX release.

To confirm the successful capping of CuS NPs, the DOX release profile from uncapped, DNA-conjugated (MSN-DNA) and CuS-capped MSNs (MSN-NH_2, MSN-DNA and MSN-DNA-CuS) were monitored at 25 °C (0-240 min) and 37 °C (Fig. 7c). At room temperature, the released DOX from three NPs were very low (<4 %). At 37 °C, the nanoparticles showed different release rates, with constantly release of DOX at similar patterns from uncapped mesoporous and DNA-conjugated MSNs, but less than 2 % DOX was released from CuS-capped MSNs. This result demonstrated the CuS capping could effectively prevent drug release at lower temperatures, and only showed thermal responsiveness at higher temperatures.

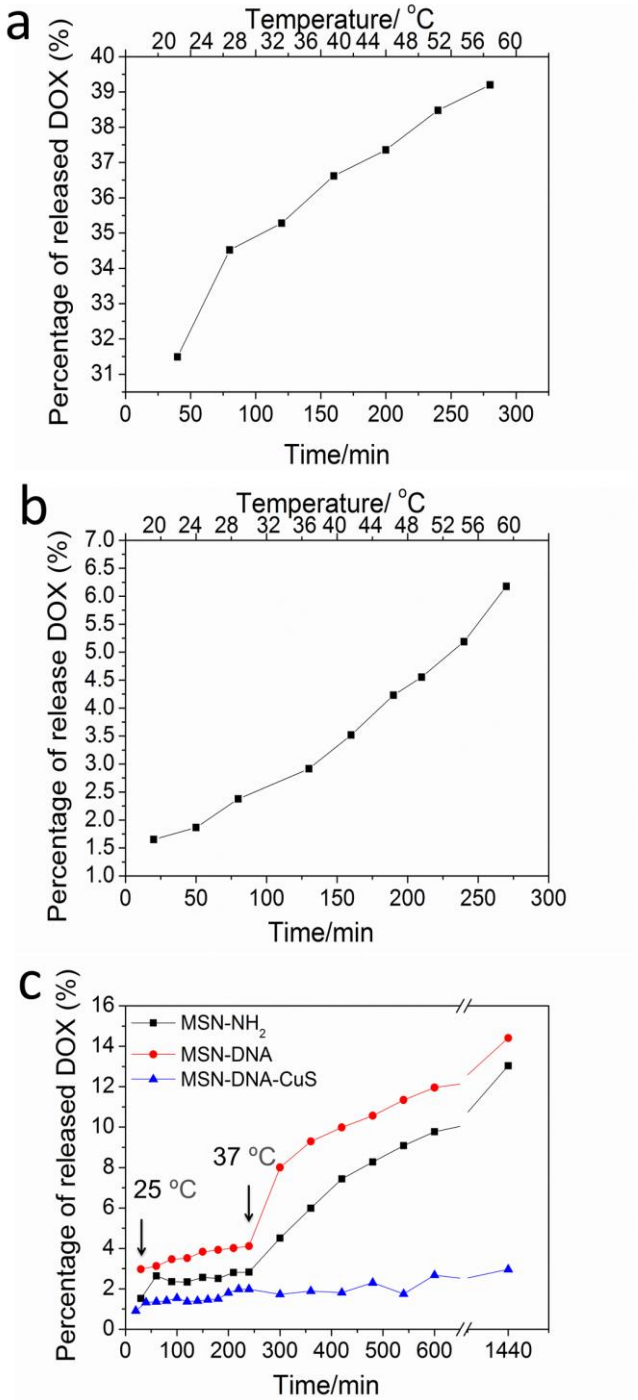

Fig. 7 (a) DOX release pattern from uncapped mesoporous silica material, in comparisonwith (b) the CuS-capped material. (c) DOX release profile from MSNs with no capping (MSN-NH_2), DNA-conjugation (MSN-DNA) and CuS-caping (MSN-DNA-CuS) at 25 ºC (0 -240 min) and 37 ºC (240-1440 min).

To monitor the temperature-responsive DOX release from MSN-DNA-CuS, the complex was placed in an incubator with increasing temperature and a 40 min hold time at each temperature (Fig. 8a). The DOX release exhibited a staircase-like profile with an obvious increase immediately after each temperature increase that slowed down in the holding phase.

When the temperature was higher than 47°C, the DOX increase rate was higher than at lower temperatures, even in the holding phase. This indicated the melting of the DNA sequence and the "opening" of the gate by the leaving of the gatekeeper. NIR irradiation of different time points also triggered DOX release, with a higher release rate after longer irradiation times (Fig. 8b).

Interestingly, glutathione (GSH) also promoted more efficient drug release (Fig. 8c). Around 20% of DOX released from MSN-DNA-CuS nanocomplex immediately after the addition of 10 mM GSH, and similar behavior could be observed in MSN-DNA nanostructures. Different from the other two, the release of DOX was in a slow enhanced pattern in MSN-NH_2 NPs. As mentioned above, since DOX was stored in MSNs via both electrostatic interactions and hydrogen bonds, GSH acted as other hydrogen bonding disturbing agent, could break the interactions between DOX and MSN,[54, 55] and accelerate the DOX release from MSN. In addition, as it has been reported that maleimide-thiol adducts can be reduced by GSH,[56] GSH may have helped to break the maleimide-thiol bond linking the hybridized DNA and MSN. The detachment of the DNA in both MSN-DNA and MSN-DNA-CuS NPs and exposure of the openings in MSNs could dramatically enhance DOX release. In the TEM images (Fig. 8d) of MSN-DNA-CuS after GSH treatment, there was CuS NPs around the MSN, but less on the surface, which confirmed the detachment of CuS NPs from MSNs.

Intracellular NIR-responsive DOX release in HeLa cells

The intracellular DOX release from the MSN-DNA-CuS complex was also studied in HeLa cells *in vitro*. After incubation of 2.5 ppm and 5.0 ppm MSN-DNA-CuS for 3 h, excess nanoparticles were completely washed out before NIR irradiation for 0, 10, 20, 30, 40 and 60 s. The heat generated from the irradiated internalized complex de-hybridized the DNA and promoted DOX release into the cell cytosol. The amount of released DOX was estimated from the DOX signal in flow cytometry (Fig. 9a and 9b). Compared with untreated cells, a right shift in the fluorescence was observed in the cells without NIR irradiation, which was attributable to the background DOX signal and the small amount of DOX that diffused from the complex in incubation. After NIR irradiation, the increased shift in the irradiated samples indicated more DOX release into the cells. Although the differences between the samples' DOX signals after irradiation of 10 to 40 s were not obvious, the signal after 60 s irradiation (especially with 5.0 ppm complex) was obviously higher, indicating the greatest DOX release.

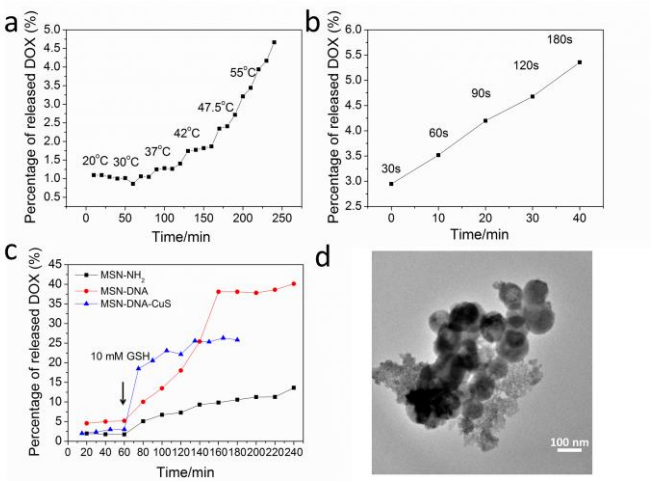

Fig. 8 The release profiles of DOX loaded MSN-DNA-CuS under different stimuli: (a) varying temperature; (b) different irradiation times with a 980 nm laser at a power density of 4 W/cm^2; (c) DOX release patterns from MSN-NH_2, MSN-DNA and MSN-DNA-CuS with 10 mM GSH added at 60 min at room temperature; and (d) a TEM image of MSN-DNA-CuS after GSH treatment.

The time-dependent DOX release of MSN-DNA-CuS was investigated at different incubation times (1 and 3 h) by confocal microscopy (Fig. 9c). The cells were exposed to the same concentration of DOX as carried by the complex as a control. With only DOX exposure, the intensity did not increase even after NIR irradiation. In comparison, stronger red DOX fluorescence was observed in NIR-irradiated cells than in untreated cells as the incubation time increased, indicated by the signal intensity below each microscopy image. Despite the increase of DOX signal, the intracellular locations of DOX also changed after NIR irradiation. In the cells after 1h exposure to complex, the red fluorescence covered nearly all the cytoplasm after irradiation, compared to the perinuclear areas before irradiation. The cells with 3 h incubation of the complex and NIR irradiation showed cell morphology changes and ruptured cell membrane, suggesting obvious cell death. This was mainly due to the promoted DOX release rate under NIR irradiation by photothermally enhanced endosomal disruption, which has also been reported by others.[23, 32] The internalization of the nanoparticles into the cells resulted in accumulated photoablation agents in the endosome/lysosome, which may have intensified the photothermal conversion efficiency, helping to disrupt the endosome and release DOX into cytosol. In addition, the GSH inside the cells may have accelerated the DOX release by interacting with the complexes, with larger changes in longer incubations.

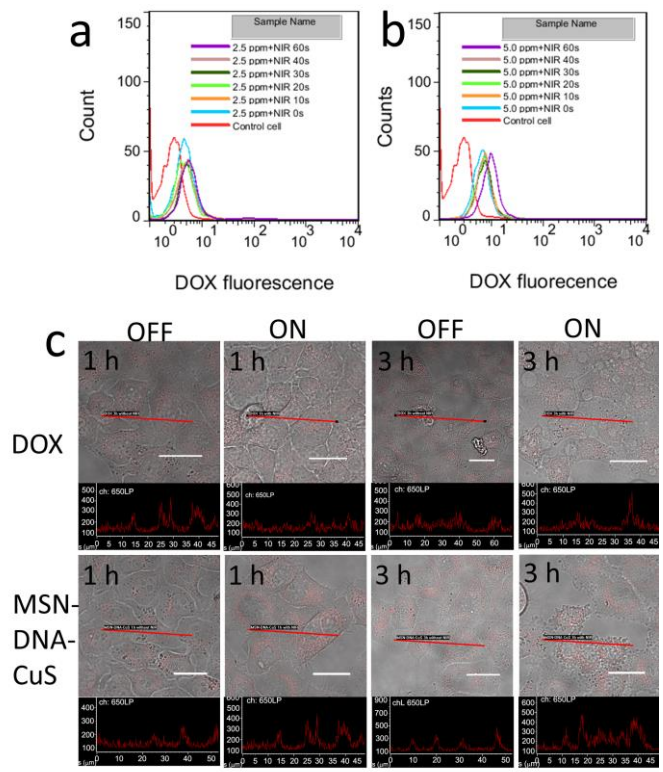

Fig. 9 NIR-responsive DOX release from MSN-DNA-CuS in HeLa cells *in vitro*. Flow cytometry histogram profile of recovered DOX fluorescence from (a) 2.5 ppm and (b) 5.0 ppm complexes after 3 h incubation with different NIR irradiation times. (c) Confocal microscopic images in HeLa cells treated with MSN-DNA-CuS in the dark (top) and under NIR irradiation (bottom) after (c, e) 1 h and (d, f) 3 h. The scale bars are 20 μM.

In vitro anticancer effect and cytotoxicity of the NIR-responsive DOX release complex

The photothermally therapeutic effect of DOX-loaded MSN-DNA-CuS was investigated using a functional approach to quantify the cell viability after NIR irradiation. HeLa and MCF-7 cells were incubated with nanoparticles for 3 h, then NIR-irradiated (Fig. 10c and 10d). More than 80% of HeLa cells survived 30 s of NIR irradiation at a power density of 4 W/cm^2. Cells exposed to CuS NPs at the same concentration as in MSN-DNA-CuS were used as controls for MSN-DNA-CuS photoablation. In the dark condition, the DOX-loaded complex showed better anticancer effects than the CuS NPs. In both cases the cytotoxicity increased as the concentration increased. The great anticancer effect was due to the diffusion of loaded DOX into the cells during incubation. After NIR irradiation for 10 s and 20 s, the cell viability did not decrease much, compared with the cells in the dark. However, after 30 s irradiation, less than 10% of the HeLa cells exposed to MSN-DNA-CuS survived, whereas CuS NPs was biocompatible with the HeLa cells even after irradiation. A similar anticancer effect was observed in the MCF-7 cells: less than 10% of the cells incubated with MSN-DNA-CuS survived after 30 s of irradiation.

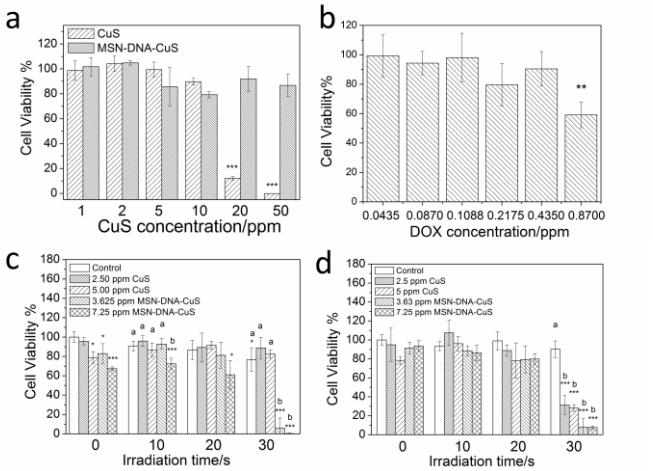

Fig. 10 Alarma Blue assay to assess (a) the cytotoxicity of MSN-DNA-CuS and CuS NPs to HeLa cells at different concentrations without NIR irradiation; (b) the cell viability of HeLa cells after exposure to DOX for 24 h; and the cell viability of (c) HeLa cells, and (d) MCF-7 cells incubated with MSN-DNA-CuS and CuS NPs, then NIR-irradiated for different times. Data are means ± S.D. $N = 3$. Bars with asterisk significant difference from control (*$p < 0.05$, **$p < 0.01$, ***$p < 0.001$; ANOVA, Tukey's test). Bars bearing different lettering are significantly different from group control ($p < 0.05$, ANOVA, Tukey's test).

There may be a critical time point between 20 s and 30 s, after which cell viability decreases dramatically. The cell viability of HeLa cells after sole DOX exposure for 24 h was used to compare the effect of different NIR-irradiation times (Fig. 10b). The DOX loading capacity was calculated to be 98.18 mg/g in MSN-NH_2. It was estimated that 0.87 ppm total DOX was loaded in 7.25 ppm MSN-DNA-CuS. Comparing the cell viability in Fig. 10b and 10c suggests that DOX played a partial role in killing the cancer cells and that the NIR irradiation enhanced this effect.

The differences in the anticancer or cell-killing effects of the MSN-DNA-CuS and CuS NPs were caused by several reasons. First, the MSN-DNA-CuS was more positively charged than the CuS NPs, leading to more accumulated nanoparticles in the cell endosomes/lysosomes. Second, the gravitational "sedimentation effect" of the silica nanoparticles caused more MSN-DNA-CuS to be deposited on the bottom of the plate, causing it to be taken up at a higher rate.[57, 58] The higher CuS uptake from the MSN-DNA-CuS was proved by the analysis of the Cu concentration in HeLa cells with ICP-OES (Fig. 11). Larger portions of the initial nanoparticles were internalized and higher Cu concentrations were observed in the HeLa cells incubated with MSN-DNA-CuS than with CuS. Third, the photothermal conversion efficiency of the complex was higher than that of CuS NPs, as shown in Fig. 6, leading to a higher localized temperature, which killed more cancer cells. Fourth, the NIR irradiation could trigger DOX release via inducing endosomal disruption, as evident by previous reports.[32, 59] Since DOX is known to cause DNA damage by mechanisms including binding to DNA and inhibiting the topoisomerase II,[60] the higher released DNA could increase the anti-cancer effect.

As the potential nonspecific toxicity of the carrier is always a great concern when using nanomaterials for drug delivery, the cytotoxicity of MSN-DNA-CuS was also evaluated (Fig. 10a). Lower concentrations of CuS NPs (1-10 ppm) were biocompatible with the HeLa cells, whereas higher amounts exhibited toxic effects. MSN-DNA-CuS was biocompatible with the cells, as more than 80% of the cells survived. The higher toxicity of CuS might come from its extremely small size and the toxicity of Cu^{2+} after internalization into the cells, due to its pre-oxidant activity and protein-binding effects.[61, 62]

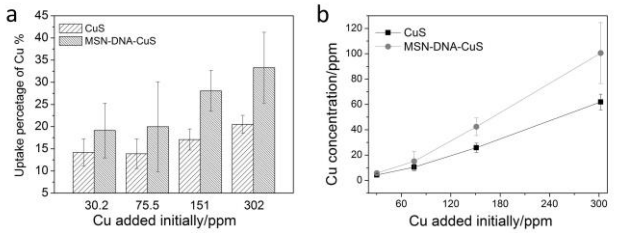

Fig. 11 Cellular uptake of Cu from CuS and MSN-DNA-CuS at different initial concentrations after 24 h exposure in HeLa cell line: (a) percentage of Cu inside the cells, compared with the initial concentration; and (b) Cu concentrations in the cell lysate.

Finally, the cell viability of the HeLa cells was evaluated at different time points after the addition of 7.25 ppm MSN-DNA-CuS with 20 s and 30 s irradiation (Fig. 12). The cell viabilities of the untreated and 20 s irradiated cells were similar at every time point. However, after 30 s irradiation 1 h after adding the nanoparticles, most of the cells were killed. The nanoparticles may not have internalized efficiently after only 1 h.[63, 64] However, the DNA may have been degraded after longer incubations inside the endosomes/lysosomes, reducing the NIR irradiation effect.

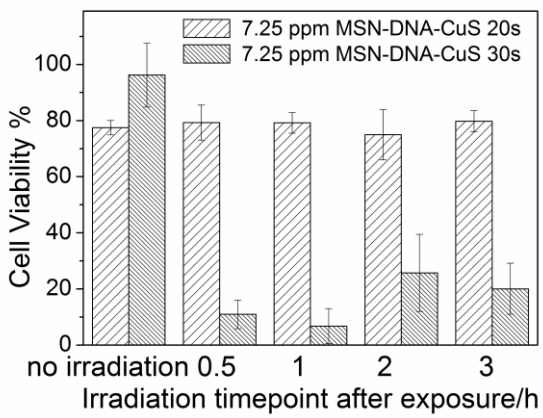

Fig. 12 Cell viability of HeLa cells after the addition of 7.25 ppm MSN-DNA-CuS and irradiation at different time points, with AlamaBlue assayed 24 h later.

Conclusions

We designed and synthesized a NIR-responsive and photothermally triggered drug delivery system, MSN-DNA-CuS, for a combinational treatment including both photothermal therapy and chemotherapy. Different from other CuS-capped MSN systems, this novel system enables reversible CuS capping even after NIR irradiation. In addition, the nanocomplex has biocompatibility and great photothermal cytotoxicity in both HeLa and MCF-7 cells. DOX release from MSN-DNA-CuS could be easily triggered by high temperature, NIR irradiation as well as GSH treatment. The multi-model drug delivery system showed higher anti-cancer effect compared to any of the single approach. This study successfully demonstrated that the MSN-DNA-CuS drug delivery system is temperature, photothermally controllable and GSH-responsive. Due to the advantages, it is a promising therapeutic agent for cancer treatment in many biological systems.

Acknowledgements

This work was financially supported by the Hong Kong PhD Fellowship to Zhang Lei and a grant from the National Natural Science Foundation of China (21173179, EE11761).

Notes and references

[a]Department of Chemistry, The Chinese University of Hong Kong, Sha Tin, N.T., Hong Kong SAR, China.
[b] School of Life Sciences, The Chinese University of Hong Kong, Sha Tin, N.T., Hong Kong SAR, China.
[#] Corresponding author.

1. C.-Y. Lai, B. G. Trewyn, D. M. Jeftinija, K. Jeftinija, S. Xu, S. Jeftinija and V. S. Y. Lin, *Journal of the American Chemical Society*, 2003, **125**, 4451-4459.
2. S. Giri, B. G. Trewyn, M. P. Stellmaker and V. S. Y. Lin, *Angewandte Chemie International Edition*, 2005, **44**, 5038-5044.
3. H. Kim, S. Kim, C. Park, H. Lee, H. J. Park and C. Kim, *Advanced Materials*, 2010, **22**, 4280-4283.
4. C. A. Hunt, R. MacGregor and R. Siegel, *Pharm Res*, 1986, **3**, 333-344.
5. L. E. Gerweck and K. Seetharaman, *Cancer Research*, 1996, **56**, 1194-1198.
6. J. Lai, B. P. Shah, E. Garfunkel and K.-B. Lee, *ACS Nano*, 2013, **7**, 2741-2750.
7. J. T. Robinson, S. M. Tabakman, Y. Liang, H. Wang, H. Sanchez Casalongue, D. Vinh and H. Dai, *Journal of the American Chemical Society*, 2011, **133**, 6825-6831.
8. N. K. Mal, M. Fujiwara, Y. Tanaka, T. Taguchi and M. Matsukata, *Chemistry of Materials*, 2003, **15**, 3385-3394.
9. E. Aznar, R. Casasús, B. García-Acosta, M. D. Marcos, R. Martínez-Máñez, F. Sancenón, J. Soto and P. Amorós, *Advanced Materials*, 2007, **19**, 2228-2231.
10. W. Fang, J. Yang, J. Gong and N. Zheng, *Advanced Functional Materials*, 2012, **22**, 842-848.
11. C. Wang, H. Xu, C. Liang, Y. Liu, Z. Li, G. Yang, L. Cheng, Y. Li and Z. Liu, *ACS Nano*, 2013, **7**, 6782-6795.
12. S. Dhar, Z. Liu, J. Thomale, H. Dai and S. J. Lippard, *Journal of the American Chemical Society*, 2008, **130**, 11467-11476.
13. Z. Liu, K. Chen, C. Davis, S. Sherlock, Q. Cao, X. Chen and H. Dai, *Cancer research*, 2008, **68**, 6652-6660.
14. A. Schlossbauer, J. Kecht and T. Bein, *Angewandte Chemie International Edition*, 2009, **48**, 3092-3095.
15. N. Mas, A. Agostini, L. Mondragón, A. Bernardos, F. Sancenón, M. D. Marcos, R. Martínez-Máñez, A. M. Costero, S. Gil, M.

Merino-Sanjuán, P. Amorós, M. Orzáez and E. Pérez-Payá, *Chemistry – A European Journal*, 2013, **19**, 1346-1356.
16. C. Park, H. Kim, S. Kim and C. Kim, *Journal of the American Chemical Society*, 2009, **131**, 16614-16615.
17. C. R. Thomas, D. P. Ferris, J.-H. Lee, E. Choi, M. H. Cho, E. S. Kim, J. F. Stoddart, J.-S. Shin, J. Cheon and J. I. Zink, *Journal of the American Chemical Society*, 2010, **132**, 10623-10625.
18. J.-H. Lee, J.-t. Jang, J.-s. Choi, S. H. Moon, S.-h. Noh, J.-w. Kim, J.-G. Kim, I.-S. Kim, K. I. Park and J. Cheon, *Nature Nanotechnology*, 2011, **6**, 418-422.
19. S. Wu, X. Huang and X. Du, *Angewandte Chemie International Edition*, 2013, **52**, 5580-5584.
20. Y. Cai, H. Pan, X. Xu, Q. Hu, L. Li and R. Tang, *Chemistry of Materials*, 2007, **19**, 3081-3083.
21. S.-F. Lee, X.-M. Zhu, Y.-X. J. Wang, S.-H. Xuan, Q. You, W.-H. Chan, C.-H. Wong, F. Wang, J. C. Yu, C. H. K. Cheng and K. C.-F. Leung, *ACS Applied Materials & Interfaces*, 2013, **5**, 1566-1574.
22. R. Weissleder, *Nature biotechnology*, 2001, **19**, 316-316.
23. G. B. Braun, A. Pallaoro, G. Wu, D. Missirlis, J. A. Zasadzinski, M. Tirrell and N. O. Reich, *ACS Nano*, 2009, **3**, 2007-2015.
24. M. A. Patel, H. Yang, P. L. Chiu, D. D. T. Mastrogiovanni, C. R. Flach, K. Savaram, L. Gomez, A. Hemnarine, R. Mendelsohn, E. Garfunkel, H. Jiang and H. He, *ACS Nano*, 2013, **7**, 8147-8157.
25. Z. Li, C. Wang, L. Cheng, H. Gong, S. Yin, Q. Gong, Y. Li and Z. Liu, *Biomaterials*, 2013, **34**, 9160-9170.
26. Y. Li, W. Lu, Q. Huang, C. Li and W. Chen, *Nanomedicine*, 2010, **5**, 1161-1171.
27. M. Zhou, R. Zhang, M. Huang, W. Lu, S. Song, M. P. Melancon, M. Tian, D. Liang and C. Li, *Journal of the American Chemical Society*, 2010, **132**, 15351-15358.
28. Q. Tian, M. Tang, Y. Sun, R. Zou, Z. Chen, M. Zhu, S. Yang, J. Wang, J. Wang and J. Hu, *Advanced Materials*, 2011, **23**, 3542-3547.
29. M. S. Yavuz, Y. Cheng, J. Chen, C. M. Cobley, Q. Zhang, M. Rycenga, J. Xie, C. Kim, K. H. Song and A. G. Schwartz, *Nature materials*, 2009, **8**, 935-939.
30. W. Li, X. Cai, C. Kim, G. Sun, Y. Zhang, R. Deng, M. Yang, J. Chen, S. Achilefu and L. V. Wang, *Nanoscale*, 2011, **3**, 1724-1730.
31. Z. Liu, J. T. Robinson, X. Sun and H. Dai, *Journal of the American Chemical Society*, 2008, **130**, 10876-10877.
32. H. Kim, D. Lee, J. Kim, T.-i. Kim and W. J. Kim, *ACS Nano*, 2013, **7**, 6735-6746.
33. L. Guo, D. D. Yan, D. Yang, Y. Li, X. Wang, O. Zalewski, B. Yan and W. Lu, *ACS Nano*, 2014, **8**, 5670-5681.
34. K. Dong, Z. Liu, Z. Li, J. Ren and X. Qu, *Advanced Materials*, 2013, **25**, 4452-4458.
35. F. Tang, L. Li and D. Chen, *Advanced Materials*, 2012, **24**, 1504-1534.
36. F. Pu, X. Liu, X. Yang, Z. Liu, J. Ren, S. Wang and X. Qu, *ChemPlusChem*, 2013, **78**, 656-662.
37. Y. Chen, H. Chen and J. Shi, *Advanced Materials*, 2013, **25**, 3144-3176.
38. X. Liu, F. Fu, K. Xu, R. Zou, J. Yang, Q. Wang, Q. Liu, Z. Xiao and J. Hu, *Journal of Materials Chemistry B*, 2014, **2**, 5358-5367.
39. L. Wu, M. Wu, Y. Zeng, D. Zhang, A. Zheng, X. Liu and J. Liu, *Nanotechnology*, 2015, **26**, 025102.
40. W. Zhang, Z. Guo, D. Huang, Z. Liu, X. Guo and H. Zhong, *Biomaterials*, 2011, **32**, 8555-8561.
41. M. Grün, I. Lauer and K. K. Unger, *Advanced Materials*, 1997, **9**, 254-257.
42. L. Zhang, Y. Li and J. C. Yu, *Journal of Materials Chemistry B*, 2014, **2**, 452-470.
43. D. Fullston, D. Fornasiero and J. Ralston, *Colloids and Surfaces A: Physicochemical and Engineering Aspects*, 1999, **146**, 113-121.
44. D.-G. Kim, E. Koyama, H. Tokuhisa, N. Koshizaki and Y. D. Kim, *Appl. Phys. A*, 2008, **92**, 263-266.
45. A. Steinbrück, A. Csaki, K. Ritter, M. Leich, J. M. Köhler and W. Fritzsche, *Journal of Biophotonics*, 2008, **1**, 104-113.
46. I. Tokareva and E. Hutter, *Journal of the American Chemical Society*, 2004, **126**, 15784-15789.
47. E. Ruiz-Hernandez, A. Baeza and M. a. Vallet-Regí, *ACS Nano*, 2011, **5**, 1259-1266.
48. K. P. Kalyanikutty, M. Nikhila, U. Maitra and C. N. R. Rao, *Chemical Physics Letters*, 2006, **432**, 190-194.
49. D. K. Roper, W. Ahn and M. Hoepfner, *The Journal of Physical Chemistry C*, 2007, **111**, 3636-3641.
50. L. Yuan, Q. Tang, D. Yang, J. Z. Zhang, F. Zhang and J. Hu, *The Journal of Physical Chemistry C*, 2011, **115**, 9926-9932.
51. R. J. Sturgeon and S. G. Schulman, *Journal of Pharmaceutical Sciences*, 1977, **66**, 958-961.
52. R. E. Yanes and F. Tamanoi, *Therapeutic Delivery*, 2012, **3**, 389-404.
53. F. Balas, M. Manzano, P. Horcajada and M. Vallet-Regí, *Journal of the American Chemical Society*, 2006, **128**, 8116-8117.
54. P. Yousefpour, F. Atyabi, E. V. Farahani, R. Sakhtianchi and R. Dinarvand, *International journal of nanomedicine*, 2011, **6**, 1487-1496.
55. Y. Tian, L. Bromberg, S. N. Lin, T. Alan Hatton and K. C. Tam, *Journal of Controlled Release*, 2007, **121**, 137-145.
56. A. D. Baldwin and K. L. Kiick, *Bioconjugate Chemistry*, 2011, **22**, 1946-1953.
57. M. Arsianti, M. Lim, C. P. Marquis and R. Amal, *Langmuir*, 2010, **26**, 7314-7326.
58. S. Zhu, H. Lu, J. Xiang, K. Tang, B. Zhang, M. Zhou, C. Tan and G. Li, *Chin.Sci.Bull.*, 2002, **47**, 654-658.
59. S. Goenka, V. Sant and S. Sant, *Journal of Controlled Release*, 2014, **173**, 75-88.
60. G. Minotti, P. Menna, E. Salvatorelli, G. Cairo and L. Gianni, *Pharmacological reviews*, 2004, **56**, 185-229.
61. M. E. Letelier, S. Sánchez-Jofré, L. Peredo-Silva, J. Cortés-Troncoso and P. Aracena-Parks, *Chemico-Biological Interactions*, 2010, **188**, 220-227.
62. M. E. Letelier, A. M. Lepe, M. Faúndez, J. Salazar, R. Marín, P. Aracena and H. Speisky, *Chemico-Biological Interactions*, 2005, **151**, 71-82.
63. E. B. Gyenge, X. Darphin, A. Wirth, U. Pieles, H. Walt, M. Bredell and C. Maake, *Journal of Nanobiotechnology*, 2011, **9**, 32.

64. M. Ekkapongpisit, A. Giovia, C. Follo, G. Caputo and C. Isidoro, *International journal of nanomedicine*, 2012, **7**, 4147.